RETRIEVAL AUGMENTED TIME SERIES FORECASTING

Anonymous authors
Paper under double-blind review

ABSTRACT

Time series forecasting uses historical data to predict future trends, leveraging the relationships between past observations and available features. In this paper, we propose, RAFT, a retrieval-augmented time series forecasting method to provide sufficient inductive biases and complement the model's learning capacity. When forecasting the subsequent time frames, we directly retrieve historical data candidates from the training dataset with patterns most similar to the input, and utilize the future values of these candidates alongside the inputs to obtain predictions. This simple approach augments the model's capacity by externally providing information about past patterns via retrieval modules. Our empirical evaluations on eight benchmark datasets show that RAFT consistently outperforms contemporary baselines, an average win ratio of 86% for multivariate forecasting and 80% for univariate forecasting tasks.

1 INTRODUCTION

Time series forecasting has a wide range of impactful applications and domains such as for climate modeling (Zhu & Shasha, 2002), energy (Martín et al., 2010), economics (Granger & Newbold, 2014), traffic flow (Chen et al., 2001), and user behavior (Benevenuto et al., 2009). By providing accurate forecasts, it helps make critical data-driven decisions and policies.

Over the past decade, deep learning models such as CNNs (Bai et al., 2018; Borovykh et al., 2017) and RNNs (Hewamalage et al., 2021) have proven their effectiveness in capturing patterns of change in historical observations, leading to the development of various deep learning models tailored for time series forecasting. Especially, the advent of attention-based Transformers (Vaswani et al., 2017) has made a significant impact on the time series domain. The architecture has shown to be effective in modeling dependencies between inputs, resulting in variants like Informer (Zhou et al., 2021), AutoFormer (Wu et al., 2021), and FedFormer (Zhou et al., 2022). Additionally, recent methods utilize time series decomposition (Wang et al., 2023), which isolates trends or seasonal patterns, and multi-periodicity analysis which involves downsampling/upsampling of the series at various periods (Lin et al., 2024; Wang et al., 2024). Furthermore, lightweight models like multi-layer perceptrons (MLP) have demonstrated strong performance along with these decomposition techniques and multi-periodicity analysis (Chen et al., 2023; Zeng et al., 2023; Zhang et al., 2022).

This paper examines a critical open question in time-series forecasting: "do current models possess the necessary inductive biases and learning capacity to extract generalizable patterns from training data and achieve high accuracy?" Many existing models operate under assumptions of i.i.d. data, potentially limiting their ability to generalize. Real-world time series exhibit complex, non-stationary patterns with varying periods and shapes. These patterns may lack inherent temporal correlation and arise from non-deterministic processes, resulting in infrequent repetitions and diverse distributions (Kim et al., 2021). This raises concerns about the effectiveness of models in extrapolating from such infrequent patterns. Moreover, the advantages of indiscriminately memorizing all patterns, including noisy and uncorrelated ones, are questionable in terms of both generalizability and efficiency (Weigend et al., 1995).

We show an advancement in time-series forecasting models by expanding the models' capacity (implicitly via the trained weights) to learn patterns. We directly provide external information about historical patterns that are complex to learn, as a way of bringing relevant information via the input to reduce the burden on the forecasting model. Inspired by the retrieval-augmented generation (RAG) approaches used in large language models (Lewis et al., 2020), our method retrieves similar

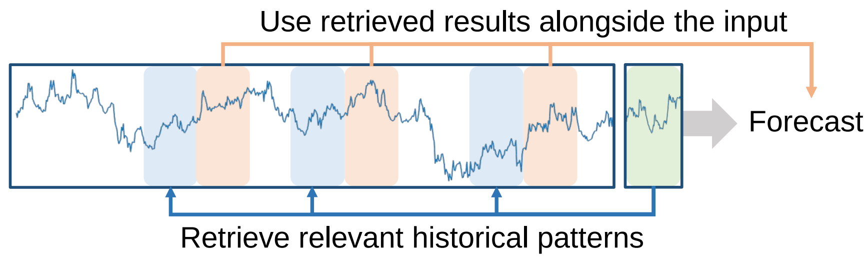

Figure 1: Illustration of a motivating example of retrieval in time-series forecasting.

historical patterns from the training dataset based on given inputs and utilizes them along with the model's learned knowledge to forecast the next time frame (see Figure 1). Our new approach, Retrieval-Augmented Forecasting of Time-series (RAFT), offers two key advantages: First, by directly utilizing retrieved information, the useful patterns from the past become explicitly available at inference time, rather than utilizing them via the learned information in model weights. The learning hence covers patterns that lack temporal correlation or do not share common characteristics with other patterns, thereby reducing the learning burden and enhancing the generalizability. Second, even if a pattern rarely appears in the historical data and is difficult for the model to memorize, the retrieval module allows the model to easily leverage the historical patterns when they reappear (Miller et al., 2024; Laptev et al., 2017).

We demonstrate that the proposed judiciously-designed inductive bias, implemented through a simple retrieval module, enables a straightforward MLP architecture to achieve strong forecasting performance. Inspired by existing literature that downsamples series at various period intervals (Lin et al., 2024; Wang et al., 2024), RAFT also generates multiple series by downsampling the given series at different periods and attaches a retrieval module to each series. This allows effectively capturing both short-term and long-term patterns for more accurate forecasting. As demonstrated on eight time-series benchmark datasets, RAFT outperforms other contemporary baselines with an average win ratio of 86% for multivariate forecasting and 80% for univariate forecasting tasks. Overall, our contributions can be summarized as follows:

- We propose a retrieval-augmented time series forecasting method, RAFT, which retrieves observations with similar temporal patterns from the training dataset and effectively leverage retrieved patterns for future predictions.
- Our empirical studies on eight different benchmark datasets show that RAFT achieves higher performance with an average win ratio of 86% for multivariate and 80% for univariate forecasting compared to other contemporary baselines.
- We further explore the scenarios where retrieval modules can be beneficial for forecasting by conducting analyses using synthetic and real-world benchmark datasets.

2 Related Work

2.1 Deep learning for time-series forecasting

A large body of research employs deep learning for time-series forecasting. Existing methods can be broadly categorized based on the employed architecture. Prior to the advent of Transformers (Vaswani et al., 2017), CNNs were commonly used to extract temporally local information from input time series through kernels (Bai et al., 2018; Borovykh et al., 2017), or RNNs with their recurrent structures (Hewamalage et al., 2021). Following the advent of Transformers, several approaches emerged to better tailor the Transformer architecture for time-series forecasting. For example, LogTrans (Li et al., 2019) used a convolutional self-attention layer, while Informer (Zhou et al., 2021) employed a ProbSparse attention module along with a distilling technique to efficiently reduce network size. Both Autoformer (Wu et al., 2021) and FedFormer (Zhou et al., 2022) decomposed time series into components like trend and seasonal patterns for prediction.

Despite advancements in Transformer-based models, (Zeng et al., 2023) reported that even a simple linear model can achieve strong forecasting performance. Subsequently, lightweight MLP-based time-series models in terms of both forecasting latency and training cost benefits, such as TiDE (Das et al., 2023), TSMixer (Chen et al., 2023), and TimeMixer (Wang et al., 2024), were introduced. These models utilize various approaches such as series decomposition similar to Transformer-based studies (Zeng et al., 2023) or introduced multi-periodicity analysis by downsampling or upsampling the series at various period intervals (Lin et al., 2024), to accurately extract the relevant information from time-series for MLPs to effectively fit on them. Recently, several studies have constructed a large time-series databases to build large foundation models, achieving strong zero-shot and few-shot performance (Das et al., 2024; Woo et al., 2024).

Our proposed RAFT is based on a simple MLP architecture, following simplicity and efficiency motivations. Through the retrieval module, the model retrieves patterns most similar to the current prediction from the training dataset, allowing it to reference past patterns for future predictions without the burden of memorizing all temporal patterns during training.

2.2 Retrieval augmented models

A typical retrieval-augmented model operates as follows: (1) Given an input, it retrieves instances relevant to the input from an accessible dataset, such as the training data or an external corpus, and (2) it combines the input with the retrieved instances to make a model prediction. One actively researched area that employs this scheme is the natural language domain, particularly in retrieval-augmented generation (RAG) (Lewis et al., 2020; Guu et al., 2020). RAG retrieves document chunks from external corpora that are relevant to the input task, helping large language models (LLMs) generate responses related to the task without hallucination (Shuster et al., 2021; Borgeaud et al., 2022). This not only supplements the LLM's limited prior knowledge but also enables the LLM to handle complex, knowledge-intensive tasks more effectively by providing additional information from the retrieved documents (Gao et al., 2023).

Beyond natural language processing, retrieval-augmented models have also been used to solve structured data problems. The simplest example is the K-nearest neighbor model (Zhang, 2016). Other approaches have introduced kernel-based neighbor methods (Nader et al., 2022), prototype-based approaches (Arik & Pfister, 2020), or considered all training samples as retrieved instances (Kossen et al., 2021). More recently, models leveraging attention-like mechanisms have incorporated the similarity between retrieved instances and the input into the prediction, achieving superior performance compared to traditional deep tabular models (Gorishniy et al., 2024). There also exists a method that has explored the potential of retrieving similar entities in time-series forecasting, involving multiple time series entities (Iwata & Kumagai, 2020; Yang et al., 2022).

In this paper, we aim to demonstrate that retrieval can be effective, even when applied to time-series data. Similar to how RAG supplements LLMs with additional information for knowledge-intensive tasks, our approach seeks to reduce the learning complexity in time-series forecasting. Instead of forcing the model to learn every possible complex pattern, the retrieval module provides information that simplifies the learning process.

3 Method

3.1 Overview

Problem formulation. Given a time series $\mathbf{S} \in \mathbb{R}^{C \times T}$ of length T with C observed variates (i.e., channels), RAFT utilizes historical observation $\mathbf{x} \in \mathbb{R}^{C \times L}$ and the entire time series $\mathbf{S}$ to predict future values $\mathbf{y} \in \mathbb{R}^{C \times F}$ that is close to the actual future values $\mathbf{y}_0 \in \mathbb{R}^{C \times F}$. L denotes look-back window size and F denotes forecasting window size.

Given an input $\mathbf{x}$, RAFT utilizes a retrieval module to find the most relevant patch from $\mathbf{S}$. Then, the subsequent patches of the relevant patch are retrieved as additional information for forecasting. The retrieval process follows an attention-like structure, where the importance weights are calculated based on the similarity between the input and the patches, and the retrieved patches are aggregated through a weighted sum (Sec. 3.2). The main difference of our model from attention-based forecasting models, such as transformers, lies in its ability to retrieve relevant data from the

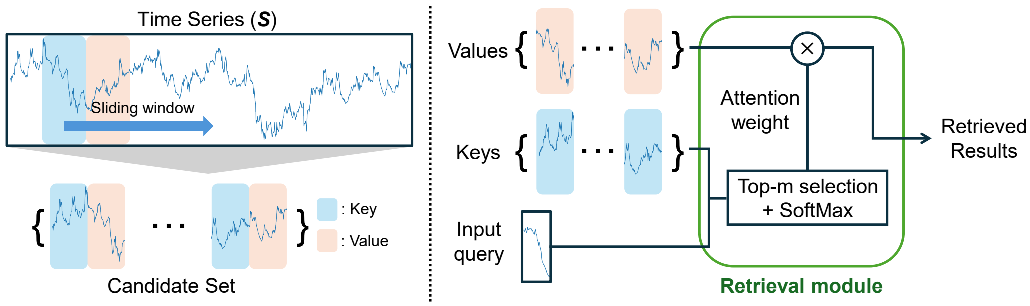

Figure 2: Illustration of retrieval module architecture. First, we consider consecutive time frames from the entire time series $\mathbf{S}$ as key-value pairs and construct a candidate set using a sliding window approach. Given an input time series as the query, the retrieval module computes the similarity between the query and the keys in the candidate set that do not overlap temporally. Based on the similarity, the top-m candidates are selected, and attention weights are calculated via SoftMax. The final result is obtained through a weighted sum of the corresponding values.

entire time series rather than relying on a fixed lookback window. Since the time series shows distinct characteristics across periods, we utilize the retrieval modules into multiple periods. RAFT generates multiple time series by downsampling the time series $\mathbf{S}$ with different periods and applies the retrieval module to each time series. The retrieval results from multiple series are processed through linear projection and aggregated by summation. Finally, the input and the aggregated retrieval result are concatenated and passed through a linear model to produce the final prediction (Sec. 3.3). Details of each component are described below.

3.2 Retrieval Module Architecture

We transform the time series $\mathbf{S}$ to be appropriate for the retrieval. First, we find all *key* patches within $\mathbf{S}$ that are to be compared with given $\mathbf{x} \in \mathbb{R}^{C \times L}$. Using the sliding window method of stride 1[1], we extract patches of window size L and define this collection as $\mathcal{K} = \{\mathbf{k}_1, ..., \mathbf{k}_{T-(L+F)+1}\}$, where i indicates the the starting time step of the patch $\mathbf{k}_i \in \mathbb{R}^{C \times L}$. Note that any patch that overlaps with the given x must be excluded from $\mathcal{K}$ during training phase. Then, we find all *value* patches that sequentially follows each key patch $\mathbf{k}_i \in \mathcal{K}$ in the time series. We define the collection of value patches as $\mathcal{V} \in \{\mathbf{v}_1, ..., \mathbf{v}_{T-(L+F)+1}\}$, where each $\mathbf{v}_i \in \mathbb{R}^{C \times F}$ sequentially follows after $\mathbf{k}_i$ in the time series.

After preparation of key patch set $\mathcal{K}$ and value patch set $\mathcal{V}$ for retrieval, we use the input $\mathbf{x}$ as a *query* to retrieve similar key patches along with their corresponding value patches with following steps. We first account for the distributional deviation between the query, key, and value patches used in the retrieval process. Let us define $\mathbf{x} = \{\mathbf{x}^t\}_{t \in \{1,...,L\}}$, where $\mathbf{x}^t \in \mathbb{R}^C$ denotes the values of C variates at t-th time step within the input $\mathbf{x}$ (i.e., $\mathbf{x}^t = \{x_1^t, ..., x_C^t\}$). Inspired by existing literature (Zeng et al., 2023), we treat the final time step value in each patch as an offset and subtract this value from the patch as a form of preprocessing to make the patterns more meaningful to compare:

$$\hat{\mathbf{x}} = \{\mathbf{x}^t - \mathbf{x}^L\}_{t \in \{1,...,L\}}, \tag{1}$$

where $\hat{\mathbf{x}}$ represent the input queries with the offset subtracted. Similarly, we subtract offset from all key patches $\mathbf{k}_i \in \mathcal{K}$ and $\mathbf{v}_i \in \mathcal{V}$, denoting them as $\hat{\mathbf{k}}_i \in \hat{\mathcal{K}}$ and $\hat{\mathbf{v}}_i \in \hat{\mathcal{V}}$, respectively. Then, we calculate the similarity ρ_i between given $\hat{\mathbf{x}}$ and all key patches in $\hat{\mathcal{K}}$ using similarity function s:

$$\rho_i = s(\hat{\mathbf{x}}, \hat{\mathbf{k}}_i), \quad \hat{\mathbf{k}}_i \in \hat{\mathcal{K}}. \tag{2}$$

Here, we use Pearson correlation as the similarity function s, instead of other measures, to exclude the effects of scale variations and value offsets in the time series, focusing on capturing the increas-

[1]The stride can be adjusted according to the demand of computational efficiency.

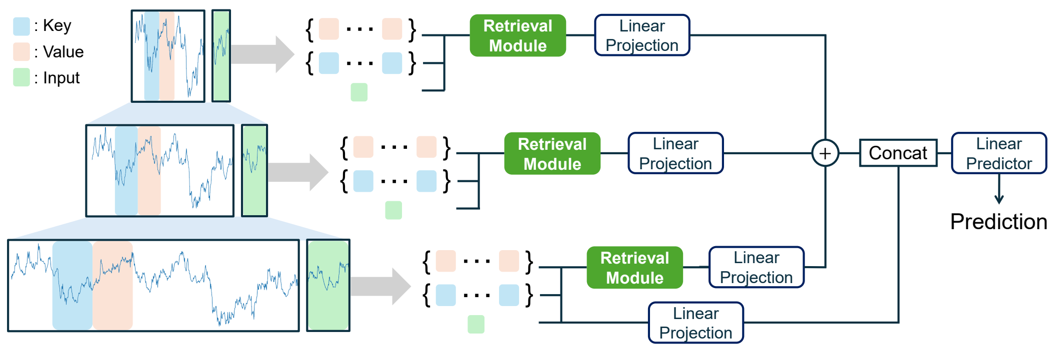

Figure 3: Illustration of the proposed architecture, RAFT. The input time series $\mathbf{x}$ and the entire past observed time series $\mathbf{S}$ are first downsampled to generate multiple series with different periods. Then, a retrieval module is applied to each series to retrieve information relevant to the current input. The retrieved results are projected to the same dimension via a linear layer, and the results from different periods are summed to aggregate the information. Finally, the input time series is concatenated with the aggregated retrieved results, and a linear layer is applied to produce the final prediction.

ing and decreasing tendencies[2]. We then retrieve the patches with top-m correlation values:

$$\mathcal{J} = \text{arg top-}m\ (\{\rho_i \mid 1 \leq i \leq |\hat{\mathcal{K}}|\}), \tag{3}$$

where $\mathcal{J}$ denotes the indices of top-m patches. Given temperature τ, we calculate the weight of value patches with following equation:

$$w_i = \begin{cases} \frac{\exp(\rho_i/\tau)}{\sum_{j \in J} \exp(\rho_j/\tau)}, & \text{if } i \in \mathcal{J} \\ 0. & \text{otherwise} \end{cases} \tag{4}$$

Note that this is equivalent to conduct SoftMax only with top-m correlation values. Finally, we obtain the final retrieval result $\tilde{\mathbf{v}} \in \mathbb{R}^{C \times F}$ as the weighted sum of value patches:

$$\tilde{\mathbf{v}} = \sum_{i \in \{1,\ldots,|\hat{\mathcal{V}}|\}} w_i \cdot \hat{\mathbf{v}}_i. \tag{5}$$

Figure 2 illustrates the architecture of our retrieval module.

3.3 Forecast with Retrieval Module

Single period. Consider the given input $\mathbf{x} \in \mathbb{R}^{C \times L}$ and the retrieved patch $\tilde{\mathbf{v}} \in \mathbb{R}^{C \times F}$. Similar to the retrieval module, we subtract the offset from $\mathbf{x}$ and define $\hat{\mathbf{x}}$ as the input with the offset removed. Next, we concatenate $f(\hat{\mathbf{x}})$ with $g(\tilde{\mathbf{v}})$, and process concatenated result through h to obtain $\hat{\mathbf{y}}$:

$$\hat{\mathbf{y}} = h(f(\hat{\mathbf{x}}) \oplus g(\tilde{\mathbf{v}})), \tag{6}$$

where linear projection f maps $\mathbb{R}^L$ to $\mathbb{R}^F$, g maps $\mathbb{R}^F$ to $\mathbb{R}^F$, h maps $\mathbb{R}^{2F}$ to $\mathbb{R}^F$, and $\oplus$ represents concatenation operation.

Multiple periods. Time series at different periods display unique characteristics – patterns in a small time window typically reveal local patterns, while patterns in a large time window might correspond to global trends. We propose extension of utilization of retrieval to consider n periods $\mathcal{P}$. For each $p \in \mathcal{P}$, we downsample the query $\mathbf{x}$, all key patches in $\mathcal{K}$, and all value patches in $\mathcal{V}$ of period 1 by average pooling with period p. This results in $\mathbf{x}^{(p)} \in \mathbb{R}^{C \times \lfloor \frac{L}{p} \rfloor}$, $\mathcal{K}^{(p)}$, and $\mathcal{V}^{(p)}$ as the respective query, key patch set, and value patch set for period p, where a key patch $\mathbf{k}_i^{(p)} \in \mathbb{R}^{C \times \lfloor \frac{L}{p} \rfloor}$ and a value patch $\mathbf{v}_i^{(p)} \in \mathbb{R}^{C \times \lfloor \frac{F}{p} \rfloor}$. Then, we conduct the retrieval process described in Sec. 3.2 using $\mathbf{x}^{(p)}$, $\mathcal{K}^{(p)}$, and $\mathcal{V}^{(p)}$, and obtain the retrieval result $\tilde{\mathbf{v}}^{(p)} \in \mathbb{R}^{C \times \lfloor \frac{F}{p} \rfloor}$ for each p. Each $\tilde{\mathbf{v}}^{(p)}$ is processed through

[2]See Appendix C.1 for comparison results with different similarity metrics.

a linear layer $g^{(p)}$ to project all retrieval results in the same embedding space, mapping $\mathbb{R}^{\lfloor \frac{F}{p} \rfloor}$ to $\mathbb{R}^F$, respectively. Finally, we concatenate $\hat{\mathbf{x}}$ with sum of linear projections and process it through linear predictor h, which replaces Eq. 6 to following equation:

$$\hat{\mathbf{y}} = h(f(\hat{\mathbf{x}}) \oplus \sum_{p \in \mathcal{P}} g^{(p)}(\tilde{\mathbf{v}}^{(p)})) \tag{7}$$

Denoting $\hat{\mathbf{y}}^t$ as the value at the t-th time step within $\hat{\mathbf{y}}$, we restore the original offset by adding $\mathbf{x}^L$ to $\hat{\mathbf{y}}$, resulting in the final forecast $\mathbf{y}$:

$$\mathbf{y} = \{\hat{\mathbf{y}}^t + \mathbf{x}^L\}_{t \in \{1,\ldots,F\}}. \tag{8}$$

We train the model by minimizing the following MSE loss $\mathcal{L}$:

$$\mathcal{L} = \text{MSE}(\mathbf{y},\ \mathbf{y}_0) \tag{9}$$

Figure 3 illustrates our model's forecasting process with multiple periods of retrieval.

4 Experiments

We evaluate RAFT across multiple time-series benchmark datasets for the forecasting task. We analyze how our proposed retrieval module contributes to performance improvement in time series forecasting, and in which scenarios retrieval is particularly beneficial. Due to space constraints, the full results, visualizations, and additional analyses of our model are provided in the Appendix.

4.1 Experimental settings

Datasets. We consider ten different benchmark datasets, each with a diverse range of variates, dataset lengths, and frequencies: (1-4) The ETT dataset contains 2 years of electricity transformer temperature data, divided into four subsets—ETTh1, ETTh2, ETTm1, and ETTm2 (Zhou et al., 2021); (5) The Electricity dataset records household electric power consumption over approximately 4 years (Trindade, 2015); (6) The Exchange dataset includes the daily exchange rates of eight countries over 27 years (1990–2016) (Lai et al., 2018); (7) The Illness dataset includes the weekly ratio of patients with influenza-like illness over 20 years (2002-2021)[3]; (8) The Solar dataset contains 10-minute solar power forecasts collected from power plants in 2006 (Liu et al., 2022a); (9) The Traffic dataset contains hourly road occupancy rates on freeways over 48 months[4]; and (10) The Weather dataset consists of 21 weather-related indicators in Germany over one year[5]. A summary of the datasets is provided in the Appendix A.

Baselines. We compare against 9 contemporary time-series forecasting baselines, including: (1) Autoformer (Wu et al., 2021), (2) Informer (Zhou et al., 2021), (3) Stationary (Liu et al., 2022b), (4) Fedformer (Zhou et al., 2022), and (5) PatchTST (Nie et al., 2023), all of which use Transformer-based architectures; (6) DLinear (Zeng et al., 2023), which are lightweight models with simple linear architectures; (7) MICN (Wang et al., 2023), which leverages both local features and global correlations through a convolutional structure; (8) TimesNet (Wu et al., 2023), which utilizes Fourier Transformation to decompose time-series data within a modular architecture; and (9) TimeMixer (Wang et al., 2024), which utilizes decomposition and multi-periodicity for forecasting.

Implementation details. RAFT employs the retrieval module with following detailed settings. The periods are set to $\{1, 2, 4\}$ ($n = 3$), following existing literature (Wang et al., 2024), and the temperature τ is set to 0.1. Batch size is set to 32. The initial learning rate, number of patches used in retrieval (m), and look back window size (L) are determined via grid search based on performance on the validation set, following the prior work (Wang et al., 2024). For fair comparison, hyperparameter tuning was performed for both our model and all baselines using the validation set. The learning rate is chosen from 1e-5 to 0.05, look back window size from $\{96, 192, 336, 720\}$, and the number of patches used in retrieval m from $\{1, 5, 10, 20\}$. The chosen values of each setting are presented in the Appendix B. For implementation, we referred to the publicly available time-series

[3] https://gis.cdc.gov/grasp/fluview/fluportaldashboard.html
[4] https://pems.dot.ca.gov/
[5] https://www.bgc-jena.mpg.de/wetter/

Table 1: Comparison of RAFT and baseline methods across 10 datasets using MSE. For all datasets except Illness, results are averaged over forecasting horizons of 96, 192, 336, and 720. For the Illness dataset, forecasting horizons of 24, 36, 48, and 60 are used. Best performances are bolded, and our framework's performances, when second-best, are underlined.

Methods	RAFT	TimeMixer	PatchTST	TimesNet	MICN	DLinear	FEDformer	Stationary	Autoformer	Informer
ETTh1	**0.420**	0.447	0.516	0.495	0.475	0.461	0.498	0.570	0.496	1.040
ETTh2	**0.359**	0.364	0.391	0.414	0.574	0.563	0.437	0.526	0.450	4.431
ETTm1	**0.348**	0.381	0.406	0.400	0.423	0.404	0.448	0.481	0.588	0.961
ETTm2	**0.254**	0.275	0.290	0.291	0.353	0.354	0.305	0.306	0.327	1.410
Electricity	**0.160**	0.182	0.216	0.193	0.196	0.225	0.214	0.193	0.227	0.311
Exchange	0.441	**0.386**	0.564	0.416	0.315	0.643	1.195	0.461	1.447	2.478
Illness	2.097	2.024	**1.480**	2.139	2.664	2.169	2.847	2.077	3.006	5.137
Solar	<u>0.231</u>	**0.216**	0.287	0.403	0.283	0.330	0.328	0.350	0.586	0.331
Traffic	**0.434**	0.484	0.529	0.620	0.593	0.625	0.610	0.624	0.628	0.764
Weather	<u>0.241</u>	**0.240**	0.265	0.251	0.268	0.265	0.309	0.288	0.338	0.634

repository (TSLib)[6]. For all experiments, the average results from three runs are reported, with each experiment conducted on a single NVIDIA A100 40GB GPU.

Evaluation. We consider two metrics for evaluation: MSE and MAE. We varied the forecasting horizon length to measure performance (i.e., $F = 96$, 192, 336, 720), and each experiment setting was run with three different random seeds to compute the average results. For the Illness dataset, forecasting horizons of 24, 36, 48, and 60 are used, following the prior work (Nie et al., 2023; Wang et al., 2024). The evaluation was conducted in multivariate settings, where both the input and forecasting target have multiple channels.

4.2 Experimental results on forecasting benchmarks

Table 1 presents comparisons between the performance of time series forecasting methods and RAFT. The results represent the average MSE performance evaluated across different forecasting horizon lengths. We observe that our model consistently outperforms other contemporary baselines on average, supporting the effectiveness of retrieval in time series forecasting. Full results and comparisons using a different evaluation metric (i.e., MAE) are provided in Appendix H.

5 Discussions

In this section, we explore scenarios where retrieval shows substantial advantage by empirically analyzing its effect, using both benchmark datasets and synthetic time series datasets.

5.1 Better retrieval results lead to better performance.

Two criteria are important for our retrieval method to enhance the forecasting performance. First, the value patches $\mathcal{V}$ identified through the similarity between the input query $\mathbf{x}$ and key patches $\mathcal{K}$ should closely match the actual future value $\mathbf{y}_0$ which sequentially follows the input query. Second, the model should efficiently leverage the information in the value patches for forecasting. From these, we can draw the insight that higher similarity between input query and key patches (i.e., key similarity) will lead to the higher similarity between the actual value and value patches (i.e., value similarity), eventually resulting in better performance.

Figure 4 presents the correlation analysis conducted on the ETTh1 dataset. Figure 4a shows that retrieving key patches with higher similarity leads to value patches that are more closely aligned with the actual future value. Figure 4b illustrates that the value patches with greater similarity to the actual future values tend to improve RAFT's performance more significantly. This trend is also consistent across datasets; datasets with higher key similarity show higher value similarity, resulting in larger performance gains. Spearman's correlation coefficient validate this trend, showing a correlation of 0.60 between key similarity and value similarity, and a correlation of -0.54 between

[6]https://github.com/thuml/Time-Series-Library

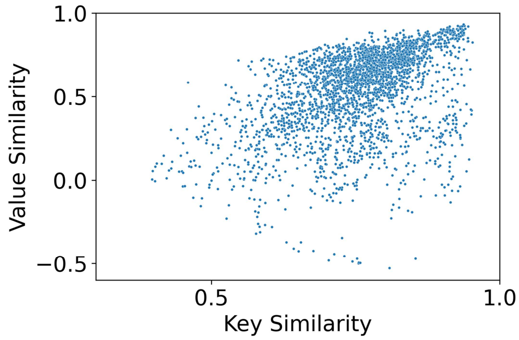

(a) Scatter plot of key and value similarity

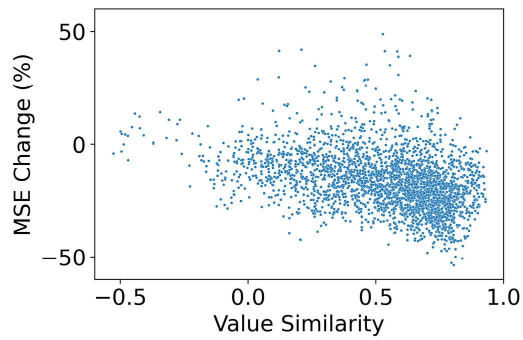

(b) Scatter plot of value similarity and MSE change (%)

Figure 4: Analysis of the correlation between (a) the key similarity and value similarity, and (b) the value similarity and model performance changes measured by MSE (%). Key similarity refers to the average similarity between input query ($\mathbf{x}$) and all retrieved key patches ($\mathcal{K}$). Value similarity refers to the average similarity between actual future value ($\mathbf{y}_0$) and all retrieved value patches ($\mathcal{V}$). The analysis is conducted on the ETTh1 dataset.

value similarity and performance gain across datasets. The negative correlation with performance is due to the use of MSE as the metric (lower the better). These results demonstrate that better retrieval results from the retrieval module lead to improved performance of RAFT.

5.2 Retrieval is particularly helpful when rare patterns repeat.

RAFT can complement scenarios where a particular pattern does not frequently appear in the training dataset, making it difficult for the model to memorize. By utilizing retrieved information, the model can overcome this challenge. To analyze this effect, we conducted experiments using synthetic time series datasets.

Synthetic data generation with autoregressive model. The synthetic time series was created by combining three different components. Two of these components represent trend and seasonality, which exhibit long-term consistent patterns throughout the entire time series. The third component represents event-based short-term patterns. To generate the trend and seasonality components, we synthesized sinusoidal functions with varying periods, amplitudes, and offsets. On the other hand, the short-term patterns were generated using an autoregressive model. Specifically, the value of the next time step was determined by the previous 20 time steps, following the equation below:

$$x_t = \sum_{i=1}^{20} \varphi_i x_{t-i} + \epsilon_t, \tag{10}$$

where φ_i represents the parameters in the autoregressive model, and ϵ_t is the noise. The parameter values and noise are sampled from a uniform distribution. The length of the short-term pattern was set to 200. To examine whether retrieval is effective for rare patterns, we created three different short-term patterns and varied their frequency of occurrence (i.e., rarity) in the training dataset. To eliminate other potential confounding factors, we varied the trend and seasonality components and randomized the order of the short-term patterns during repeated experiments. We then measured and compared the average forecasting accuracy (i.e., MSE) when each pattern appeared in the test set, with both the input and the forecasting horizon lengths fixed at 96. Additional details and example figures of the synthetic dataset can be found in Figure 5a and in the Appendix F.

Results. Table 2 presents the number of occurrences of the short-term patterns and the corresponding performance of RAFT with and without retrieval. Note that, in this experiment, we did not consider multiple periods in order to isolate the effect of retrieval, so RAFT without retrieval has an identical structure to the NLinear baseline (Zeng et al., 2023). The results show that our model, utilizing retrieval, consistently outperformed the model without retrieval on the synthetic dataset; 9.2∼14.7% increase in performance depending on the pattern occurrences. Notably, as the pattern occurrences decreased, the reduction in MSE was more significant. When we also visualize

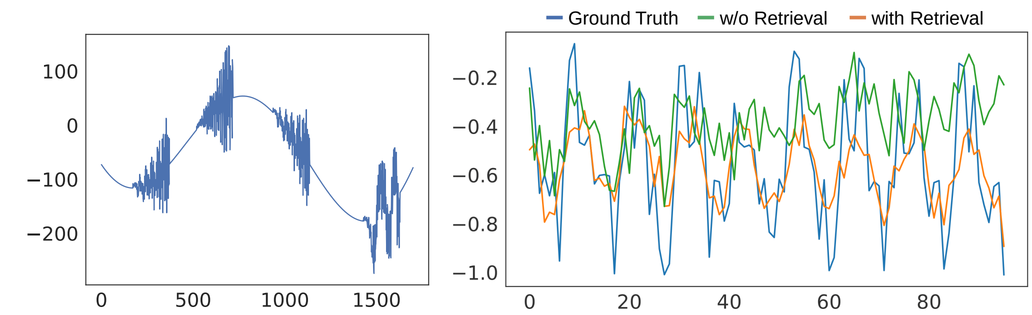

(a) Example plot of the synthetic time series

(b) Predictions with and without retrieval module

Figure 5: Visualization of a synthetic time series with short-term patterns and the corresponding predictions over the rare short-term pattern from models with and without the retrieval module. MSE of predictions in this example without retrieval is 0.087, while with retrieval, it improves to 0.035.

Table 2: Analysis between forecasting accuracy and the rarity of the pattern over the synthetic time series with an autoregressive model. Forecasting accuracy was evaluated using MSE, averaged across 120 different time series and short-term patterns. The numbers in parentheses indicate the ratio by which the MSE decreases when retrieval is appended.

Pattern occurrences	1	2	4
RAFT without Retrieval	0.2590	0.2310	0.2344
RAFT with Retrieval	0.2209 (-14.7%)	0.2064 (-10.7%)	0.2128 (-9.2%)

the predictions of models with and without retrieval modules over the rare pattern (see Figure 5b), the model utilizing retrieval aligns well with the pattern's periodicity and offset during forecasting, while the model relying solely on learning fails to capture these aspects. This suggests that the model struggles to learn rare patterns, and the retrieval module effectively complements this deficiency.

5.3 Retrieval is helpful when patterns are temporally less correlated.

If short-term patterns are very similar across time, there's less unique information for the model to learn, making it easier to achieve accurate predictions. On the other hand, if the short-term patterns in time series data are similar to a random walk without any specific temporal correlation, the model would need to memorize all changes within short-term pattern for accurate forecasting. Based on this hypothesis, we expect the retrieval module to be especially helpful when patterns are temporally less correlated, as retrieval can easily detect similarities between patterns that temporal correlation alone cannot capture. We again use the synthetic dataset for validation.

Synthetic data generation with random walk model. Instead of generating short-term patterns using the autoregressive model as before, we utilize random walk-based change patterns, following the equation:

$$x_t = x_{t-1} + \epsilon_t. \tag{11}$$

The step size for the walk ϵ_t was sampled from a uniform distribution within the range of [-20, 20]. The generated short-term patterns were then inserted into the training data, as in the previous synthetic time-series approach.

Results. Table 3 shows the results of applying the same experiment as in Table 2, but with different synthetic time-series data. Again, the retrieval module improves performance across all cases, particularly for rare patterns. Furthermore, the performance improvement is more significant for temporally less correlated patterns (16.0∼31.5% decrease of MSE depending on pattern occurrences), compared to temporally more correlated ones shown in Table 2 (9.2∼14.7%). This confirms that the proposed retrieval module is more beneficial when dealing with temporally less correlated or near-random patterns that are more challenging for the model to learn.

Table 3: Forecasting accuracy over the rarity of the pattern. Synthetic time series with random walk based patterns (temporally less correlated) is used. Forecasting accuracy was evaluated using MSE, averaged across 120 different time series and short-term patterns. The numbers in parentheses indicate the ratio by which the MSE decreases when retrieval is appended.

Pattern occurrences	1	2	4
RAFT without retrieval	0.2694	0.2649	0.1894
RAFT with retrieval	0.1845 (-31.5%)	0.1818 (-31.4%)	0.1592 (-16.0%)

6 Conclusion

In this paper, we introduce RAFT, a time-series forecasting method that leverages retrieval from training data to augment the input. Our retrieval module lessens the model to absorb all unique patterns in its weights, particularly those that lack temporal correlation or do not share common characteristics with other patterns. This overall is demonstrated as an effective inductive bias for deep learning architectures for time-series. Our extensive evaluations on numerous real-world and synthetic datasets confirm that RAFT achieves performance improvements over contemporary baselines. As various retrieval-based models are being proposed, there remains room for improvement in retrieval techniques specifically tailored for time-series data (beyond the simple approaches used), including determining when, where, and how to apply retrieval based on dataset characteristics and capture more complex similarity measures that depend on nonlinear and nonstationary characteristics. Our work is expected to open new avenues in the time-series forecasting field through the use of retrieval-augmented approaches.

References

Sercan O Arik and Tomas Pfister. Protoattend: Attention-based prototypical learning. *Journal of Machine Learning Research*, 21(210):1–35, 2020.

Shaojie Bai, J Zico Kolter, and Vladlen Koltun. An empirical evaluation of generic convolutional and recurrent networks for sequence modeling. *arXiv preprint arXiv:1803.01271*, 2018.

Fabrício Benevenuto, Tiago Rodrigues, Meeyoung Cha, and Virgílio Almeida. Characterizing user behavior in online social networks. In *Proceedings of the 9th ACM SIGCOMM Conference on Internet Measurement*, pp. 49–62, 2009.

Sebastian Borgeaud, Arthur Mensch, Jordan Hoffmann, Trevor Cai, Eliza Rutherford, Katie Millican, George Bm Van Den Driessche, Jean-Baptiste Lespiau, Bogdan Damoc, Aidan Clark, et al. Improving language models by retrieving from trillions of tokens. In *International conference on machine learning*, pp. 2206–2240. PMLR, 2022.

Anastasia Borovykh, Sander Bohte, and Cornelis W Oosterlee. Conditional time series forecasting with convolutional neural networks. *arXiv preprint arXiv:1703.04691*, 2017.

Chao Chen, Karl Petty, Alexander Skabardonis, Pravin Varaiya, and Zhanfeng Jia. Freeway performance measurement system: mining loop detector data. *Transportation research record*, 1748 (1):96–102, 2001.

Si-An Chen, Chun-Liang Li, Sercan O Arik, Nathanael Christian Yoder, and Tomas Pfister. Tsmixer: An all-mlp architecture for time series forecast-ing. *Transactions on Machine Learning Research*, 2023.

Abhimanyu Das, Weihao Kong, Andrew Leach, Shaan Mathur, Rajat Sen, and Rose Yu. Long-term forecasting with tide: Time-series dense encoder. *arXiv preprint arXiv:2304.08424*, 2023.

Abhimanyu Das, Weihao Kong, Rajat Sen, and Yichen Zhou. A decoder-only foundation model for time-series forecasting. In *Forty-first International Conference on Machine Learning*, 2024.

Yunfan Gao, Yun Xiong, Xinyu Gao, Kangxiang Jia, Jinliu Pan, Yuxi Bi, Yi Dai, Jiawei Sun, and Haofen Wang. Retrieval-augmented generation for large language models: A survey. *arXiv preprint arXiv:2312.10997*, 2023.

Yury Gorishniy, Ivan Rubachev, Nikolay Kartashev, Daniil Shlenskii, Akim Kotelnikov, and Artem Babenko. Tabr: Tabular deep learning meets nearest neighbors. In *The Twelfth International Conference on Learning Representations*, 2024.

Clive William John Granger and Paul Newbold. *Forecasting economic time series*. Academic press, 2014.

Kelvin Guu, Kenton Lee, Zora Tung, Panupong Pasupat, and Mingwei Chang. Retrieval augmented language model pre-training. In *International conference on machine learning*, pp. 3929–3938. PMLR, 2020.

Hansika Hewamalage, Christoph Bergmeir, and Kasun Bandara. Recurrent neural networks for time series forecasting: Current status and future directions. *International Journal of Forecasting*, 37 (1):388–427, 2021.

Tomoharu Iwata and Atsutoshi Kumagai. Few-shot learning for time-series forecasting. *arXiv preprint arXiv:2009.14379*, 2020.

Taesung Kim, Jinhee Kim, Yunwon Tae, Cheonbok Park, Jang-Ho Choi, and Jaegul Choo. Reversible instance normalization for accurate time-series forecasting against distribution shift. In *International Conference on Learning Representations*, 2021.

Jannik Kossen, Neil Band, Clare Lyle, Aidan N Gomez, Thomas Rainforth, and Yarin Gal. Self-attention between datapoints: Going beyond individual input-output pairs in deep learning. *Advances in Neural Information Processing Systems*, 34:28742–28756, 2021.

Guokun Lai, Wei-Cheng Chang, Yiming Yang, and Hanxiao Liu. Modeling long-and short-term temporal patterns with deep neural networks. In *The 41st international ACM SIGIR conference on research & development in information retrieval*, pp. 95–104, 2018.

Nikolay Laptev, Jason Yosinski, Li Erran Li, and Slawek Smyl. Time-series extreme event forecasting with neural networks at uber. In *International conference on machine learning*, volume 34, pp. 1–5. sn, 2017.

Patrick Lewis, Ethan Perez, Aleksandra Piktus, Fabio Petroni, Vladimir Karpukhin, Naman Goyal, Heinrich Küttler, Mike Lewis, Wen-tau Yih, Tim Rocktäschel, et al. Retrieval-augmented generation for knowledge-intensive nlp tasks. *Advances in Neural Information Processing Systems*, 33: 9459–9474, 2020.

Shiyang Li, Xiaoyong Jin, Yao Xuan, Xiyou Zhou, Wenhu Chen, Yu-Xiang Wang, and Xifeng Yan. Enhancing the locality and breaking the memory bottleneck of transformer on time series forecasting. *Advances in neural information processing systems*, 32, 2019.

Shengsheng Lin, Weiwei Lin, Wentai Wu, Haojun Chen, and Junjie Yang. Sparsetsf: Modeling long-term time series forecasting with* 1k* parameters. In *Forty-first International Conference on Machine Learning*, 2024.

Minhao Liu, Ailing Zeng, Muxi Chen, Zhijian Xu, Qiuxia Lai, Lingna Ma, and Qiang Xu. Scinet: Time series modeling and forecasting with sample convolution and interaction. *Advances in Neural Information Processing Systems*, 35:5816–5828, 2022a.

Yong Liu, Haixu Wu, Jianmin Wang, and Mingsheng Long. Non-stationary transformers: Exploring the stationarity in time series forecasting. *Advances in Neural Information Processing Systems*, 35:9881–9893, 2022b.

Luis Martín, Luis F Zarzalejo, Jesus Polo, Ana Navarro, Ruth Marchante, and Marco Cony. Prediction of global solar irradiance based on time series analysis: Application to solar thermal power plants energy production planning. *Solar Energy*, 84(10):1772–1781, 2010.

John A Miller, Mohammed Aldosari, Farah Saeed, Nasid Habib Barna, Subas Rana, I Budak Arpinar, and Ninghao Liu. A survey of deep learning and foundation models for time series forecasting. *arXiv preprint arXiv:2401.13912*, 2024.

Youssef Nader, Leon Sixt, and Tim Landgraf. Dnnr: Differential nearest neighbors regression. In *International Conference on Machine Learning*, pp. 16296–16317. PMLR, 2022.

Yuqi Nie, Nam H Nguyen, Phanwadee Sinthong, and Jayant Kalagnanam. A time series is worth 64 words: Long-term forecasting with transformers. In *The Eleventh International Conference on Learning Representations*, 2023.

Kurt Shuster, Spencer Poff, Moya Chen, Douwe Kiela, and Jason Weston. Retrieval augmentation reduces hallucination in conversation. *arXiv preprint arXiv:2104.07567*, 2021.

Artur Trindade. ElectricityLoadDiagrams20112014. UCI Machine Learning Repository, 2015. DOI: https://doi.org/10.24432/C58C86.

Ashish Vaswani, Noam Shazeer, Niki Parmar, Jakob Uszkoreit, Llion Jones, Aidan N Gomez, Łukasz Kaiser, and Illia Polosukhin. Attention is all you need. In *Advances in Neural Information Processing Systems*, pp. 5998–6008, 2017.

Huiqiang Wang, Jian Peng, Feihu Huang, Jince Wang, Junhui Chen, and Yifei Xiao. Micn: Multi-scale local and global context modeling for long-term series forecasting. In *The eleventh international conference on learning representations*, 2023.

Shiyu Wang, Haixu Wu, Xiaoming Shi, Tengge Hu, Huakun Luo, Lintao Ma, James Y Zhang, and JUN ZHOU. Timemixer: Decomposable multiscale mixing for time series forecasting. In *The Twelfth International Conference on Learning Representations*, 2024.

Andreas S Weigend, Morgan Mangeas, and Ashok N Srivastava. Nonlinear gated experts for time series: Discovering regimes and avoiding overfitting. *International journal of neural systems*, 6 (04):373–399, 1995.

Gerald Woo, Chenghao Liu, Akshat Kumar, Caiming Xiong, Silvio Savarese, and Doyen Sahoo. Unified training of universal time series forecasting transformers. In *Forty-first International Conference on Machine Learning*, 2024.

Haixu Wu, Jiehui Xu, Jianmin Wang, and Mingsheng Long. Autoformer: Decomposition transformers with auto-correlation for long-term series forecasting. *Advances in neural information processing systems*, 34:22419–22430, 2021.

Haixu Wu, Tengge Hu, Yong Liu, Hang Zhou, Jianmin Wang, and Mingsheng Long. Timesnet: Temporal 2d-variation modeling for general time series analysis. In *The Eleventh International Conference on Learning Representations*, 2023.

Sitan Yang, Carson Eisenach, and Dhruv Madeka. Mq-retcnn: Multi-horizon time series forecasting with retrieval-augmentation. In *8th SIGKDD International Workshop on Mining and Learning from Time Series – Deep Forecasting: Models, Interpretability, and Applications*, 2022.

Ailing Zeng, Muxi Chen, Lei Zhang, and Qiang Xu. Are transformers effective for time series forecasting? In *Proceedings of the AAAI conference on artificial intelligence*, volume 37, pp. 11121–11128, 2023.

Tianping Zhang, Yizhuo Zhang, Wei Cao, Jiang Bian, Xiaohan Yi, Shun Zheng, and Jian Li. Less is more: Fast multivariate time series forecasting with light sampling-oriented mlp structures. *arXiv preprint arXiv:2207.01186*, 2022.

Zhongheng Zhang. Introduction to machine learning: k-nearest neighbors. *Annals of translational medicine*, 4(11), 2016.

Haoyi Zhou, Shanghang Zhang, Jieqi Peng, Shuai Zhang, Jianxin Li, Hui Xiong, and Wancai Zhang. Informer: Beyond efficient transformer for long sequence time-series forecasting. In *Proceedings of the AAAI conference on artificial intelligence*, volume 35, pp. 11106–11115, 2021.

Tian Zhou, Ziqing Ma, Qingsong Wen, Xue Wang, Liang Sun, and Rong Jin. Fedformer: Frequency enhanced decomposed transformer for long-term series forecasting. In *International conference on machine learning*, pp. 27268–27286. PMLR, 2022.

Yunyue Zhu and Dennis Shasha. Statstream: Statistical monitoring of thousands of data streams in real time. In *VLDB'02: Proceedings of the 28th International Conference on Very Large Databases*, pp. 358–369. Elsevier, 2002.

APPENDIX

A DATASET DETAILS

In this work, we use widely-used 10 time series datasets. The detailed information of each dataset are shown in Table 4. The dataset size is presented in (Train, Validation, Test). The targets used in the univariate setting are as follows: oil temperature for the ETTh1, ETTh2, ETTm1, ETTm2 datasets; the consumption of a client for the Electricity dataset; the exchange rate of Singapore for the Exchange Rate dataset; the weekly ratio of patients for Illness dataset; 10-minute solar power forecasts collected from power plants for the Solar dataset; the road occupancy rates measured by a sensor for the Traffic dataset; and CO_2 (ppm) for the Weather dataset.

Table 4: Basic information of datasets used for evaluation.

Dataset	# of variates	Dataset Size	Frequency
ETTh1	7	(8449, 2785, 2785)	Hourly
ETTh2	7	(8449, 2785, 2785)	Hourly
ETTm1	7	(34369, 11425, 11425)	15 min
ETTm2	7	(34369, 11425, 11425)	15 min
Electricity	321	(18221, 2537, 5165)	Hourly
Exchange Rate	8	(5120, 665, 1422)	Daily
Illness	7	(485, 2, 98)	Weekly
Solar	137	(36601, 5161, 10417)	10 min
Traffic	862	(12089, 1661, 3413)	Hourly
Weather	21	(36696, 5175, 10444)	10min

B IMPLEMENTATION DETAILS

RAFT employs a retrieval module with the following detailed settings. The periods are set to $1, 2, 4$ ($n = 3$), following existing literature (Wang et al., 2024). The temperature τ is set to 0.1. The remaining settings, including the look back window size L, the learning rate, and the number of patches used in retrieval m are determined through grid search based on validation set performance, consistent with prior work (Wang et al., 2024). The effect of hyper-parameters (L, m, τ) on the performance are analyzed in the Section C.3-C.4.

Table 5 provides the parameter settings of our model for each dataset. We observed that some parameters vary across different datasets.

Table 5: The chosen parameter values of each setting via grid search over the validation set.

	Forecasting horizon size	Look back window size	Learning rate	Number of retrievals
ETTh1	96	720	1.00E-03	20
	192	720	1.00E-02	20
	336	720	1.00E-02	20
	720	720	1.00E-04	20
ETTh2	96	720	1.00E-02	10
	192	720	1.00E-03	10
	336	720	1.00E-03	20
	720	720	1.00E-04	20
ETTm1	96	720	1.00E-02	1
	192	720	1.00E-03	20
	336	720	1.00E-03	20
	720	720	1.00E-02	20
ETTm2	96	720	1.00E-03	5
	192	720	1.00E-03	20
	336	720	1.00E-04	20
	720	720	1.00E-04	20
Electricity	96	720	1.00E-02	1
	192	720	1.00E-03	1
	336	720	1.00E-03	1
	720	720	1.00E-03	1
Exchange	96	720	1.00E-04	1
	192	720	1.00E-03	1
	336	720	1.00E-03	10
	720	720	1.00E-04	20
Illness	96	96	1.00E-02	1
	192	96	1.00E-02	1
	336	96	1.00E-02	20
	720	96	1.00E-02	20
Solar	96	720	1.00E-03	1
	192	720	1.00E-02	1
	336	720	1.00E-03	1
	720	720	1.00E-03	1
Traffic	96	720	1.00E-02	1
	192	720	1.00E-03	1
	336	720	1.00E-03	1
	720	720	1.00E-03	1
Weather	96	720	1.00E-02	1
	192	720	1.00E-03	1
	336	720	1.00E-03	1
	720	720	1.00E-03	1

C Component Analysis

In this section, we analyze the impact of each component of RAFT on performance.

C.1 Different Similarity Metrics for Retrieval

We compared RAFT using various similarity metrics, including Pearson's correlation, cosine similarity, cosine similarity with projection, and negative L2 distance. Cosine similarity with projection employs a trainable linear projection head for the input query and key vectors, respectively, and measures cosine similarity between the embeddings after projection rather than between the raw query and key. Table 6 presents the comparison results across datasets, where Pearson's correlation shows the best performance among the various similarity metrics. We also observe that the linear projection does not provide a benefit compared to measuring similarity with the raw query and key.

Table 6: Comparison of various similarity metrics with RAFT in the univariate setting.

	Pearson's Correlation	Cosine Similarity	Cosine Sim with Projection	Negative L2 Distance
ETTh1	**0.0559**	0.0561	0.0562	0.0562
ETTh2	**0.1231**	0.1235	0.1298	0.1271
ETTm1	0.0299	0.0298	**0.0294**	0.0296
ETTm2	**0.0647**	0.0649	0.0699	0.0666
Electricity	**0.3307**	0.3343	0.3981	0.3388
Exchange Rate	**0.0915**	0.0917	0.0933	0.0922
Traffic	**0.2737**	0.2773	0.2943	0.2925
Weather	0.0118	0.0129	**0.0026**	0.0278

C.2 Ablation Study on Retrieval Module

To thoroughly analyze the impact of the proposed retrieval design on performance, we conducted an ablation study on the retrieval module. The ablations were as follows: (1) Random Retrieval – Key patches are retrieved randomly, without considering similarity to the query; (2) Without Attention – When aggregating value patches, we use equal weights instead of similarity-based weights (Eq. 5); (3) Without Retrieval – Retrieval is entirely removed, leaving only the linear predictor. The experiments were conducted under identical hyper-parameter and learning settings and evaluated on multivariate forecasting tasks. Table 7 presents the MSE results for each dataset across the ablations. As shown in the results, our model with all components included consistently achieved the best performance compared to the baselines across all datasets. Notably, we observed that when retrieval was conducted randomly or without attention, performance was sometimes even worse than without retrieval, which demonstrates that retrieving relevant data is crucial for achieving high performance.

Table 7: Ablation study on retrieval module in the multivariate setting.

	ETTh1	ETTh2	ETTm1	ETTm2	Electricity	Exchange Rate	Traffic	Weather
RAFT	**0.367**	**0.276**	**0.302**	**0.164**	**0.133**	**0.091**	**0.378**	**0.165**
Random Retrieval	0.382	0.282	0.305	0.171	0.150	0.092	0.413	0.188
Without Attention	0.379	0.281	0.300	0.165	0.148	0.090	0.409	0.172
Without Retrieval	0.379	0.282	0.306	0.167	0.143	0.089	0.410	0.182

C.3 Effect of Look Back Window Size (L)

We analyze the effect of look back window size (L) on forecasting performance. Keeping all other experimental settings fixed, we varied the look back window size between 96, 192, 336, and 720 to observe performance changes. The experiments were conducted in a multivariate setting across four datasets, with the prediction length set to 96. Table 8 compares the MSE results for different look back window sizes. Consistent with prior works (Wang et al., 2024; Zeng et al., 2023), we observed that RAFT, based on a linear model, also achieves better forecasting performance as the look back window size increases.

Table 8: Comparison results over different look back window size.

Look back window size (L)	96	192	336	720
ETTh1	0.387	0.390	0.386	0.367
ETTh2	0.296	0.292	0.281	0.276
ETTm1	0.348	0.310	0.306	0.302
ETTm2	0.179	0.171	0.166	0.164

C.4 Hyper-Parameter Analysis

RAFT has two key internal model parameters. The first is the number of patches retrieved by the retrieval module, and the second is the temperature τ used in the softmax function to calculate weights. Each hyper-parameter is optimally tuned for each dataset based on the validation set. Table 9-10 below illustrates examples of performance variations (MSE) across four datasets with different hyper-parameter values. As shown, the optimal values of the hyper-parameters vary depending on the dataset.

Table 9: Effect of the number of retrievals (m) on performance.

The number of retrievals (m)	1	5	10	20
ETTh1	0.370	0.368	0.367	0.367
ETTh2	0.280	0.278	0.276	0.275
ETTm1	0.302	0.300	0.298	0.297
ETTm2	0.164	0.164	0.164	0.164

Table 10: Effect of the temperature (τ) on performance.

Temperature (τ)	0.01	0.1	1	10
ETTh1	0.383	0.367	0.378	0.381
ETTh2	0.285	0.276	0.280	0.281
ETTm1	0.303	0.302	0.300	0.304
ETTm2	0.165	0.164	0.165	0.167

D RAFT AS AN ADD-ON MODULE OVER TRANSFORMER-VARIANTS

In this paper, we demonstrate the effectiveness of the proposed retrieval module using the simple linear architecture. However, the retrieval module can be seamlessly integrated into other architectures. To explore its extensibility, we combine the retrieval module into a Transformer-based architecture, specifically AutoFormer. As shown in Table 11, our retrieval module successfully enhances the forecasting performance of the Transformer-based model, highlighting its potential for broader applicability to other architectures.

Table 11: Performance comparison between AutoFormer and AutoFormer with our proposed retrieval module. The average MSE across different forecasting horizon lengths is reported.

	ETTh1	ETTh2	ETTm1	ETTm2
Autoformer	0.496	0.450	0.588	0.327
+ Retrieval	**0.471**	**0.444**	**0.454**	**0.326**

E Computational Complexity for Retrieval

Our model incorporates a retrieval process to find similar patches in the given data. For efficient training, the retrieval process is pre-computed for the training and validation data, requiring computation only once during training. We analyzed the wall time (in seconds) for retrieval pre-computation, training, and inference on the ETTm1 dataset (see Table 12). The lookback window size was set to 720, and the forecasting horizon length was set to 96.

Table 12: Wall time for each process of RAFT over ETTm1.

	Pre-computation	Training time per epoch	Total Inference time
Wall time (sec)	42.2	7.3	1.9

The pre-computation speed for retrieval of our model is O(N^2), where N denotes the size of the time-series in the training data. To reduce this time, one approach is to increase the stride of the sliding window beyond 1, speeding up the search process. Table 13 records the changes in wall time as the stride of the sliding window increases. As the stride increases, the time required for the search process decreases significantly.

Table 13: Wall time across different number of strides over ETTm1.

Stride	1	2	4	8
Wall time for pre-computation (sec)	42.2	19.8	9.3	4.7

Lastly, we examined the impact of increasing the stride on forecasting performance. Table 14 presents the changes in MSE across four datasets (ETTh1, ETTh2, ETTm1, ETTm2) as the stride increases. While increasing the stride introduced a performance trade-off, we observed that the decrease in performance was not significant.

Table 14: MSE changes of RAFT over four datasets across the different number of strides.

Stride	1	2	4	8
ETTh1	0.367	0.379	0.381	0.383
ETTh2	0.276	0.279	0.279	0.280
ETTm1	0.302	0.298	0.299	0.300
ETTm2	0.164	0.164	0.165	0.165

F SYNTHETIC DATASET GENERATION DETAILS

The synthetic time series was created by combining three different components. Two of these components represent trend and seasonality, which exhibit long-term consistent patterns throughout the entire time series. The third component represents event-based short-term patterns. The generation details for each component are as follows:

Trend and seasonality components. To generate the trend and seasonality components, we synthesized sinusoidal functions with varying periods, amplitudes, and offsets. The total length of the time series was set to 18,000. The period of the sinusoidal function for the trend was sampled from a uniform distribution between [1000, 4000], while the period for seasonality was shorter, sampled from [500, 1000]. The amplitude of each component was randomly chosen from the ranges [200, 300] for the trend and [100, 200] for the seasonality. Offsets were sampled from the range [100, 200].

Short-term patterns from the autoregressive model. The length of each short-term pattern was set to 200. In the case of the autoregressive model, the value of the next time step was determined by the previous 20 time steps, following the equation below:

$$x_t = \sum_{i=1}^{20} \varphi_i x_{t-i} + \epsilon_t, \tag{12}$$

where φ_i represents the parameters in the autoregressive model, and ϵ_t is the noise. The parameters were sampled from a uniform distribution within [-5, 5], and the noise was sampled from a uniform distribution within [-10, 10]. The length of the short-term pattern was set to 200. To prevent the short-term patterns from producing extreme values compared to the trend and seasonal components, we clamped the values within the range [-100, 100].

Short-term patterns from the random-walk model. In the case of the random-walk model, the length of the short-term pattern was also fixed at 200. Unlike the autoregressive model, in the random-walk model, the value of the next time step depends only on the previous time step, as described by the equation:

$$x_t = x_{t-1} + \epsilon_t., \tag{13}$$

where the step size for the walk was sampled from a uniform distribution within the range of [0, 20]. Again, to prevent the short-term patterns from producing extreme values compared to the trend and seasonal components, we clamped the values within the range [-100, 100].

Finally, the trend, seasonality, and short-term patterns were combined to create the synthetic time series. Example visualizations of the autoregressive short-term pattern, the random-walk pattern, and the resulting synthetic time series can be seen in Figure 6.

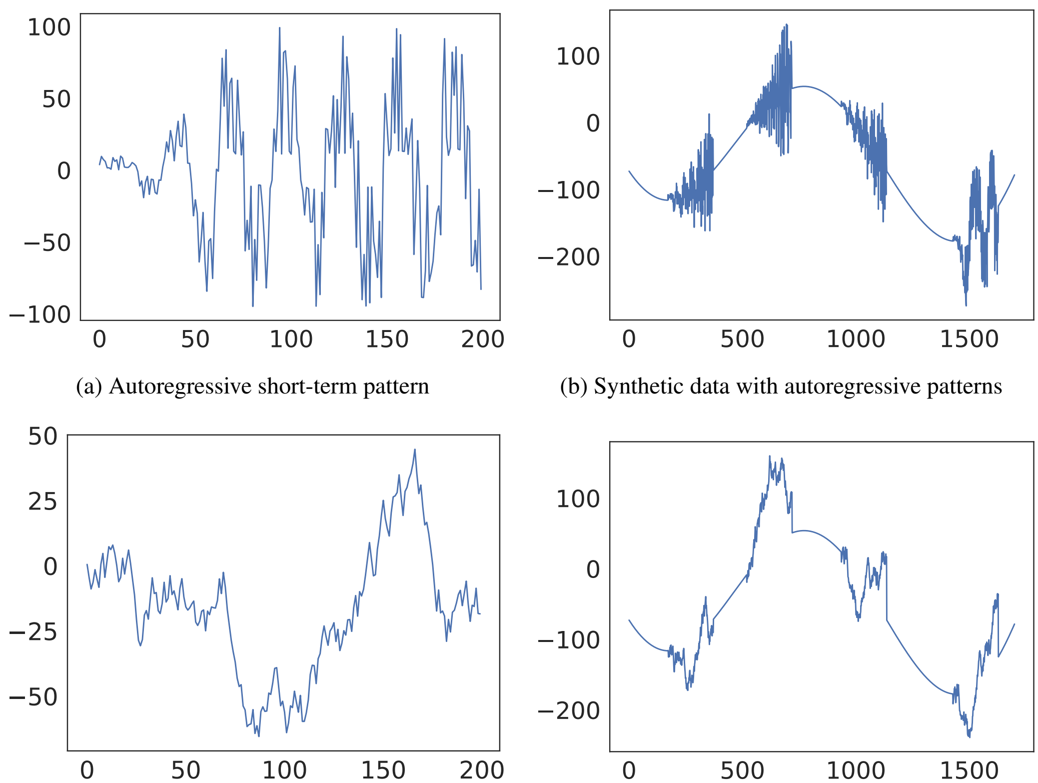

(a) Autoregressive short-term pattern

(b) Synthetic data with autoregressive patterns

(c) Random-walk short-term pattern

(d) Synthetic data with random-walk patterns

Figure 6: Visualization of an example synthetic time series with short-term patterns.

G Qualitative Analysis on Retrieval

In this section, we provide examples of our retrieval results. Figure 7-9 illustrate a comparison between the input query and the retrieved key patch, as well as a comparison between the ground truth and the retrieved value patch, with retrievals by 1, 2, and 4 periods. Note that we retrieve the key patch with the top-1 similarity and its following value patch. The results demonstrate that our retrieval module effectively delivers useful information for forecasting future predictions.

(a) Input query and retrieved key patch (period 1) (b) Ground truth and retrieved value patch (period 1)

(c) Input query and retrieved key patch (period 2) (d) Ground truth and retrieved value patch (period 2)

(e) Input query and retrieved key patch (period 4) (f) Ground truth and retrieved value patch (period 4)

Figure 7: The example of our retrieval results on ETTh1 dataset. The key patches retrieved by period 1, 2, and 4 are compared with input query in (a), (c), and (e), respectively. The value patches retrieved by period 1, 2, and 4 are compared with ground truth in (b), (d), and (f), respectively. Note that the figures in the right side sequentially follows after the figures in the left side within the time series.

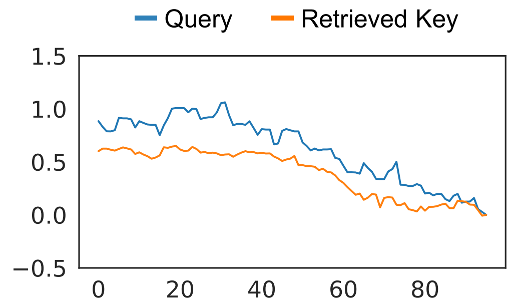

(a) Input query and retrieved key patch (period 1)

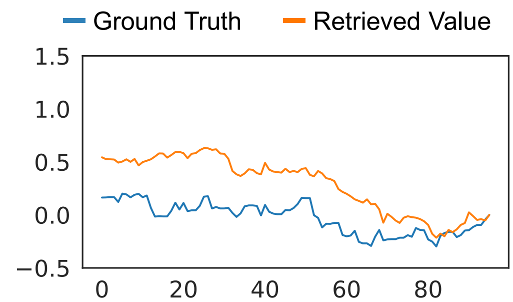

(b) Ground truth and retrieved value patch (period 1)

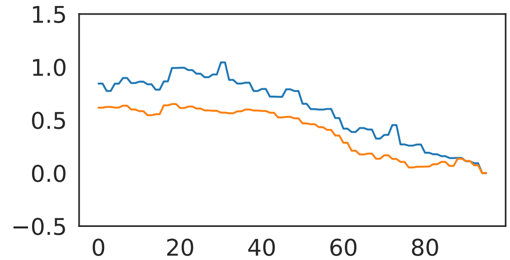

(c) Input query and retrieved key patch (period 2)

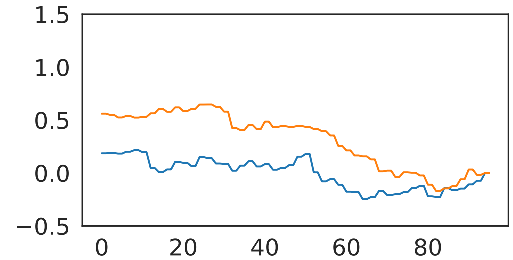

(d) Ground truth and retrieved value patch (period 2)

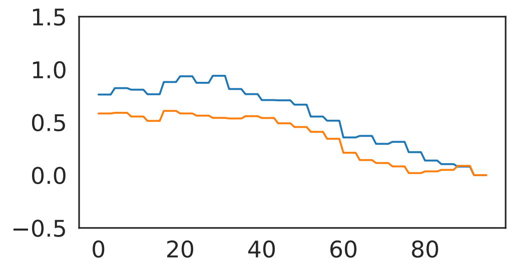

(e) Input query and retrieved key patch (period 4)

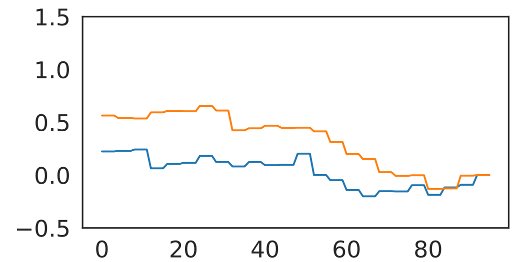

(f) Ground truth and retrieved value patch (period 4)

Figure 8: The example of our retrieval results on Exchange Rate dataset. The key patches retrieved by period 1, 2, and 4 are compared with input query in (a), (c), and (e), respectively. The value patches retrieved by period 1, 2, and 4 are compared with ground truth in (b), (d), and (f), respectively. Note that the figures in the right side sequentially follows after the figures in the left side within the time series.

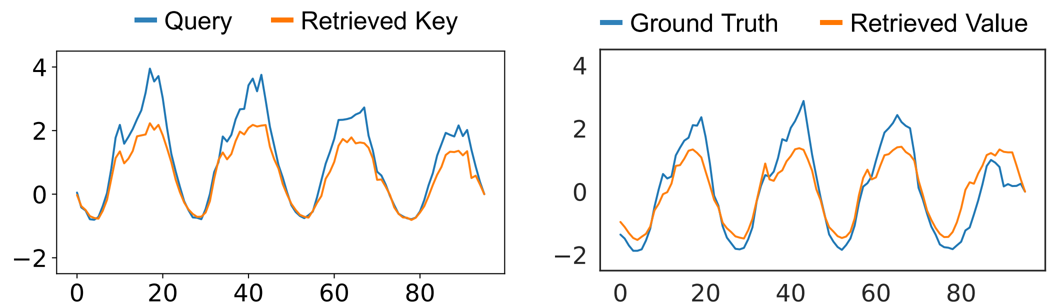

(a) Input query and retrieved key patch (period 1) (b) Ground truth and retrieved value patch (period 1)

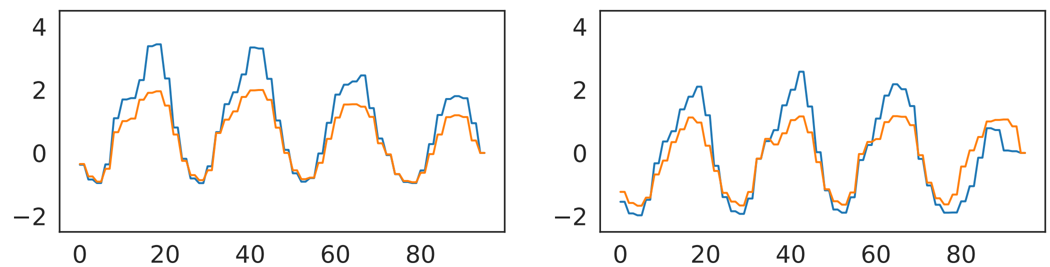

(c) Input query and retrieved key patch (period 2) (d) Ground truth and retrieved value patch (period 2)

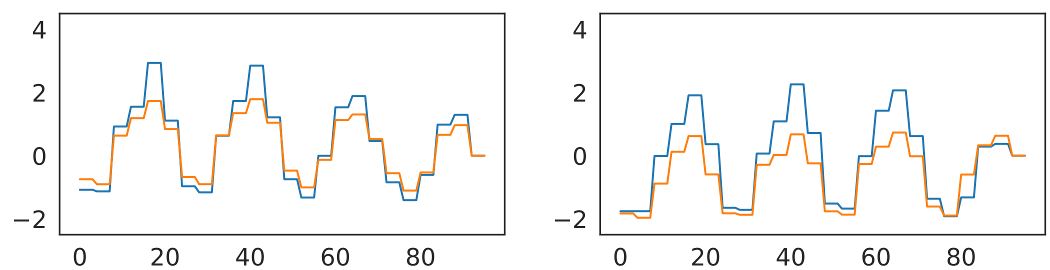

(e) Input query and retrieved key patch (period 4) (f) Ground truth and retrieved value patch (period 4)

Figure 9: The example of our retrieval results on Traffic dataset. The key patches retrieved by period 1, 2, and 4 are compared with input query in (a), (c), and (e), respectively. The value patches retrieved by period 1, 2, and 4 are compared with ground truth in (b), (d), and (f), respectively. Note that the figures in the right side sequentially follows after the figures in the left side within the time series.

H Full Results

H.1 Evaluation Results with MSE

Table 15: Full evaluation results with MSE are provided, with some baseline results excerpted from prior works (Wang et al., 2024; Nie et al., 2023).

Methods		Ours	TimeMixer	PatchTST	TimesNet	MICN	DLinear	FEDformer	Stationary	Autoformer	Informer
ETTh1	96	0.367	0.375	0.460	0.384	0.426	0.397	0.395	0.513	0.449	0.865
	192	0.411	0.429	0.512	0.436	0.454	0.446	0.469	0.534	0.500	1.008
	336	0.436	0.484	0.546	0.638	0.493	0.489	0.530	0.588	0.521	1.107
	720	0.467	0.498	0.544	0.521	0.526	0.513	0.598	0.643	0.514	1.181
	Avg	0.420	0.447	0.516	0.495	0.475	0.461	0.498	0.570	0.496	1.040
ETTh2	96	0.276	0.289	0.308	0.340	0.372	0.340	0.358	0.476	0.346	3.755
	192	0.347	0.372	0.393	0.402	0.492	0.482	0.429	0.512	0.456	5.602
	336	0.376	0.386	0.427	0.452	0.607	0.591	0.496	0.552	0.482	4.721
	720	0.436	0.412	0.436	0.462	0.824	0.839	0.463	0.562	0.515	3.647
	Avg	0.359	0.365	0.391	0.414	0.574	0.563	0.437	0.526	0.450	4.431
ETTm1	96	0.302	0.320	0.352	0.338	0.365	0.346	0.379	0.386	0.505	0.672
	192	0.329	0.361	0.390	0.374	0.403	0.382	0.426	0.459	0.553	0.795
	336	0.355	0.390	0.421	0.410	0.436	0.415	0.445	0.495	0.621	1.212
	720	0.406	0.454	0.462	0.478	0.489	0.473	0.543	0.585	0.671	1.166
	Avg	0.348	0.381	0.406	0.400	0.423	0.404	0.448	0.481	0.588	0.961
ETTm2	96	0.164	0.175	0.183	0.187	0.197	0.193	0.203	0.192	0.255	0.365
	192	0.219	0.237	0.255	0.249	0.284	0.284	0.269	0.280	0.281	0.533
	336	0.275	0.298	0.309	0.321	0.381	0.382	0.325	0.334	0.339	1.363
	720	0.359	0.391	0.412	0.408	0.549	0.558	0.421	0.417	0.433	3.379
	Avg	0.254	0.275	0.290	0.291	0.353	0.354	0.305	0.306	0.327	1.410
Electricity	96	0.133	0.153	0.190	0.168	0.180	0.210	0.193	0.169	0.201	0.274
	192	0.149	0.166	0.199	0.184	0.189	0.210	0.201	0.182	0.222	0.296
	336	0.161	0.185	0.217	0.198	0.198	0.223	0.214	0.200	0.231	0.300
	720	0.197	0.225	0.258	0.220	0.217	0.258	0.246	0.222	0.254	0.373
	Avg	0.160	0.182	0.216	0.193	0.196	0.225	0.214	0.193	0.227	0.311
Exchange	96	0.091	0.095	0.084	0.107	0.102	0.081	0.148	0.111	0.197	0.847
	192	0.205	0.201	0.180	0.226	0.172	0.157	0.271	0.219	0.300	1.204
	336	0.353	0.350	0.510	0.367	0.272	0.305	0.460	0.421	0.509	1.672
	720	1.115	0.898	1.480	0.964	0.714	0.643	1.195	1.092	1.447	2.478
	Avg	0.441	0.386	0.564	0.416	0.315	0.297	0.519	0.461	0.613	1.550
Illness	24	2.076	1.896	1.319	2.317	2.684	2.215	3.228	2.294	3.483	5.764
	36	2.183	1.928	1.579	1.972	2.667	1.963	2.679	1.825	3.103	4.755
	48	2.073	2.132	1.553	2.238	2.558	2.130	2.622	2.010	2.669	4.763
	60	2.058	2.141	1.470	2.027	2.747	2.368	2.857	2.178	2.770	5.264
	Avg	2.097	2.024	1.480	2.139	2.664	2.169	2.847	2.077	3.006	5.137
Solar	96	0.192	0.189	0.265	0.373	0.257	0.290	0.286	0.321	0.456	0.287
	192	0.247	0.222	0.288	0.397	0.278	0.320	0.291	0.346	0.588	0.297
	336	0.240	0.231	0.301	0.420	0.298	0.353	0.354	0.357	0.595	0.367
	720	0.246	0.223	0.295	0.420	0.299	0.357	0.380	0.375	0.733	0.374
	Avg	0.231	0.216	0.287	0.403	0.283	0.330	0.328	0.350	0.593	0.331
Traffic	96	0.378	0.462	0.526	0.593	0.577	0.650	0.587	0.612	0.613	0.719
	192	0.391	0.473	0.522	0.617	0.589	0.598	0.604	0.613	0.616	0.696
	336	0.402	0.498	0.517	0.629	0.594	0.605	0.621	0.618	0.622	0.777
	720	0.434	0.506	0.552	0.640	0.613	0.645	0.626	0.653	0.660	0.864
	Avg	0.402	0.485	0.529	0.620	0.593	0.625	0.610	0.624	0.628	0.764
Weather	96	0.165	0.163	0.186	0.172	0.198	0.195	0.217	0.173	0.266	0.300
	192	0.211	0.208	0.234	0.219	0.239	0.237	0.276	0.245	0.307	0.598
	336	0.260	0.251	0.284	0.246	0.285	0.282	0.339	0.321	0.359	0.578
	720	0.327	0.339	0.356	0.365	0.351	0.345	0.403	0.414	0.419	1.059
	Avg	0.241	0.240	0.265	0.251	0.268	0.265	0.309	0.288	0.338	0.634

H.2 Evaluation Results with MAE

Table 16: Full evaluation results with MAE are provided, with some baseline results excerpted from prior works (Wang et al., 2024; Nie et al., 2023).

Methods		Ours	TimeMixer	PatchTST	TimesNet	MICN	DLinear	FEDformer	Stationary	Autoformer	Informer
ETTh1	96	0.397	0.400	0.447	0.402	0.446	0.412	0.424	0.491	0.459	0.713
	192	0.427	0.421	0.477	0.429	0.464	0.441	0.470	0.504	0.482	0.792
	336	0.442	0.458	0.496	0.469	0.487	0.467	0.499	0.535	0.496	0.809
	720	0.478	0.482	0.517	0.500	0.526	0.510	0.544	0.616	0.512	0.865
	Avg	0.436	0.440	0.484	0.450	0.481	0.458	0.484	0.537	0.487	0.795
ETTh2	96	0.344	0.341	0.355	0.374	0.424	0.394	0.397	0.458	0.388	1.525
	192	0.393	0.392	0.405	0.414	0.492	0.479	0.439	0.493	0.452	1.931
	336	0.425	0.414	0.436	0.452	0.555	0.541	0.487	0.551	0.486	1.835
	720	0.473	0.434	0.450	0.468	0.655	0.661	0.474	0.560	0.511	1.625
	Avg	0.409	0.395	0.412	0.427	0.532	0.519	0.449	0.516	0.459	1.729
ETTm1	96	0.349	0.357	0.374	0.375	0.387	0.374	0.419	0.398	0.475	0.571
	192	0.367	0.381	0.393	0.387	0.408	0.391	0.441	0.444	0.496	0.669
	336	0.383	0.404	0.414	0.411	0.431	0.415	0.459	0.464	0.537	0.871
	720	0.413	0.441	0.449	0.450	0.462	0.451	0.490	0.516	0.561	0.823
	Avg	0.378	0.396	0.408	0.406	0.422	0.408	0.452	0.456	0.517	0.734
ETTm2	96	0.256	0.258	0.270	0.267	0.296	0.293	0.287	0.274	0.339	0.453
	192	0.296	0.299	0.314	0.309	0.361	0.361	0.328	0.339	0.340	0.563
	336	0.336	0.340	0.347	0.351	0.429	0.429	0.366	0.361	0.372	0.887
	720	0.392	0.396	0.404	0.403	0.522	0.525	0.415	0.413	0.432	1.338
	Avg	0.320	0.323	0.334	0.333	0.402	0.402	0.349	0.347	0.371	0.810
Electricity	96	0.232	0.247	0.296	0.272	0.293	0.302	0.308	0.273	0.317	0.368
	192	0.247	0.256	0.304	0.322	0.302	0.305	0.315	0.286	0.334	0.386
	336	0.259	0.277	0.319	0.300	0.312	0.319	0.329	0.304	0.443	0.394
	720	0.297	0.310	0.352	0.320	0.330	0.350	0.355	0.321	0.361	0.439
	Avg	0.259	0.273	0.318	0.304	0.309	0.319	0.327	0.296	0.364	0.397
Exchange	96	0.209	0.214	0.203	0.234	0.235	0.203	0.278	0.237	0.323	0.752
	192	0.324	0.320	0.302	0.344	0.316	0.293	0.380	0.335	0.369	0.895
	336	0.431	0.427	0.531	0.448	0.407	0.414	0.500	0.476	0.524	1.036
	720	0.801	0.702	0.959	0.746	0.658	0.601	0.841	0.769	0.941	1.310
	Avg	0.441	0.416	0.499	0.443	0.404	0.378	0.500	0.454	0.539	0.998
Illness	24	0.956	0.860	0.754	0.934	1.112	1.081	1.260	0.945	1.287	1.677
	36	1.008	0.910	0.870	0.920	1.068	0.963	1.080	0.848	1.148	1.467
	48	0.972	0.956	0.815	0.940	1.052	1.024	1.078	0.900	1.085	1.469
	60	0.974	0.956	0.788	0.928	1.110	1.096	1.157	0.963	1.125	1.564
	Avg	0.977	0.920	0.807	0.931	1.086	1.041	1.144	0.914	1.161	1.544
Solar	96	0.251	0.259	0.323	0.358	0.325	0.378	0.341	0.380	0.446	0.323
	192	0.323	0.283	0.332	0.376	0.354	0.398	0.337	0.369	0.561	0.341
	336	0.300	0.292	0.339	0.380	0.375	0.415	0.416	0.387	0.588	0.429
	720	0.311	0.285	0.336	0.381	0.379	0.413	0.437	0.424	0.633	0.431
	Avg	0.296	0.280	0.333	0.374	0.358	0.401	0.383	0.390	0.557	0.381
Traffic	96	0.273	0.285	0.347	0.321	0.350	0.396	0.366	0.338	0.388	0.391
	192	0.277	0.296	0.332	0.336	0.356	0.370	0.373	0.340	0.382	0.379
	336	0.282	0.296	0.334	0.336	0.358	0.373	0.383	0.328	0.337	0.420
	720	0.297	0.313	0.352	0.350	0.361	0.394	0.382	0.355	0.408	0.472
	Avg	0.282	0.298	0.341	0.336	0.356	0.383	0.376	0.340	0.379	0.416
Weather	96	0.222	0.209	0.227	0.220	0.261	0.252	0.296	0.223	0.336	0.384
	192	0.264	0.250	0.265	0.261	0.299	0.295	0.336	0.285	0.367	0.544
	336	0.302	0.287	0.301	0.337	0.336	0.331	0.380	0.338	0.395	0.523
	720	0.355	0.341	0.349	0.359	0.388	0.382	0.428	0.410	0.428	0.741
	Avg	0.286	0.272	0.286	0.294	0.321	0.315	0.360	0.314	0.382	0.548